Biochimica et Biophysica Acta 1837 (2014) 1472–1483

Contents lists available at ScienceDirect

Biochimica et Biophysica Acta

journal homepage: www.elsevier.com/locate/bbabio

Molecular dynamics study of the primary charge separation reactions in Photosystem I: Effect of the replacement of the axial ligands to the electron acceptor A_0 ☆

Georgy E. Milanovsky [a,b], Vasily V. Ptushenko [a], John H. Golbeck [c,d], Alexey Yu. Semenov [a,*], Dmitry A. Cherepanov [e,**]

[a] A.N. Belozersky Institute of Physical–Chemical Biology, Moscow State University, Moscow, Russia
[b] Faculty of Bioengineering and Bioinformatics, Moscow State University, Moscow, Russia
[c] Department of Biochemistry and Molecular Biology, The Pennsylvania State University, University Park, PA, USA
[d] Department of Chemistry, The Pennsylvania State University, University Park, PA, USA
[e] A.N. Frumkin Institute of Physical Chemistry and Electrochemistry, Russian Academy of Sciences, Moscow, Russia

ARTICLE INFO

Article history:
Received 30 October 2013
Received in revised form 3 March 2014
Accepted 5 March 2014
Available online 15 March 2014

Keywords:
Photosystem I
Molecular dynamics
Quantum chemistry
Primary reactions
Charge separation
Reorganization energy

ABSTRACT

Molecular dynamics (MD) calculations, a semi-continuum (SC) approach, and quantum chemistry (QC) calculations were employed together to investigate the molecular mechanics of ultrafast charge separation reactions in Photosystem I (PS I) of *Thermosynechococcus elongatus*. A molecular model of PS I was developed with the aim to relate the atomic structure with electron transfer events in the two branches of cofactors. A structural flexibility map of PS I was constructed based on MD simulations, which demonstrated its rigid hydrophobic core and more flexible peripheral regions. The MD model permitted the study of atomic movements (dielectric polarization) in response to primary and secondary charge separations, while QC calculations were used to estimate the direct chemical effect of the A_{0A}/A_{0B} ligands (Met or Asn in the 688/668 position) on the redox potential of chlorophylls A_{0A}/A_{0B} and phylloquinones A_{1A}/A_{1B}. A combination of MD and SC approaches was used to estimate reorganization energies λ of the primary (λ_1) and secondary (λ_2) charge separation reactions, which were found to be independent of the active branch of electron transfer; in PS I from the wild type, λ_1 was estimated to be 390 ± 20 mV, while λ_2 was estimated to be higher at 445 ± 15 mV. MD and QC approaches were used to describe the effect of substituting $Met688_{PsaA}/Met668_{PsaB}$ by $Asn688_{PsaA}/Asn668_{PsaB}$ on the energetics of electron transfer. Unlike Met, which has limited degrees of freedom in the site, Asn was found to switch between two relatively stable conformations depending on cofactor charge. The introduction of Asn and its conformation flexibility significantly affected the reorganization energy of charge separation and the redox potentials of chlorophylls A_{0A}/A_{0B} and phylloquinones A_{1A}/A_{1B}, which may explain the experimentally observed slowdown of secondary electron transfer in the $M688N_{PsaA}$ variant. This article is part of a Special Issue entitled: Photosynthesis research for sustainability: Keys to produce clean energy.

1. Introduction

Photosystem I (PS I) from cyanobacteria, algae, and higher plants is a chlorophyll (Chl) protein complex that contains low potential iron–sulfur clusters (F_A/F_B) which act as terminal electron acceptors. PS I belongs to the Type I class of photosynthetic reaction centers (RCs) and is evolutionarily close to the RCs of green sulfur bacteria and heliobacteria [1]. PS I is responsible for light-induced electron transfer from plastocyanin to ferredoxin, although, in cyanobacteria, cytochrome c_6 and flavodoxin function as alternative donors and acceptors under conditions of copper and iron limitations, respectively. The three-dimensional structure of PS I from the thermophilic cyanobacterium *Thermosynechococcus elongatus* has been solved by X-ray crystallography at a resolution of 2.5 Å [2]. In higher plants, PS I complexes are monomers, whereas in cyanobacteria they form trimers [3]. Each

Abbreviations: PS I, Photosystem I; Chl, chlorophyll; RC, reaction center; P_{700}, the primary electron donor in PS I; A_0, the primary chlorophyll electron acceptor in PS I; A_1, the secondary phylloquinone electron acceptor in PS I; An, light-harvesting antenna chlorophyll; Chl1A, Chl2A, Chl3A, Chl1B, Chl2B, Chl3B, chlorophyll molecules in PS I RC belonging to the *A* or *B* symmetric cofactor branches; A_{1A}, A_{1B}, phylloquinone molecules in PS I RC belonging to the *A* or *B* symmetric cofactor branches; N, A_0^-, A_1^-, neutral state of cofactor charging, primary charge separation state, secondary charge separation state; MD, molecular dynamics; SC, semi-continuum; QC, quantum chemistry; DFT, density functional theory

☆ This article is part of a Special Issue entitled: Photosynthesis research for sustainability: Keys to produce clean energy.

* Correspondence to: A.Y. Semenov, A.N. Belozersky Institute of Physical–Chemical Biology, Moscow State University, Leninskie Gory, Moscow 119992, Russia. Tel.: +7 495 939 3188; fax: +7 495 939 3181.
** Corresponding author. Tel.: +7 495 955 4751; fax: +7 495 952 5308.
E-mail addresses: semenov@genebee.msu.ru (A.Y. Semenov), tscherepanov@gmail.com (D.A. Cherepanov).

http://dx.doi.org/10.1016/j.bbabio.2014.03.001
0005-2728/

monomer (~300 kDa) contains one copy of 12 different protein subunits. The membrane-spanning core consists of two large subunits (products of genes *psaA* and *psaB*), which bind most of the Chl*a* molecules, 22 β-carotene molecules, two phylloquinone molecules, and an interpolypeptide [4Fe–4S] cluster F_X. The majority of 96 Chl*a* molecules function as light-harvesting antenna. The terminal [4Fe–4S] clusters F_A/F_B are bound to the peripheral stromal subunit PsaC, which has a molecular mass of ~9 kDa.

The electron transfer cofactors are located on subunits PsaA, PsaB, and PsaC, which form the core of PS I complex. The stromal subunits PsaD and PsaE do not contain redox cofactors but are necessary for the interaction of PS I with ferredoxin/flavodoxin. The primary electron donor P_{700} consists of a molecule of Chl*a* and a molecule of Chl*a*′ (Chl1A/Chl1B) and is positioned with their porphyrin planes parallel to each other (at distance of 3.6 Å) and perpendicular to the membrane plane. The X-ray analysis of PS I also revealed two Chl*a* molecules in positions corresponding to the two bacteriochlorophylls in the RC of purple bacteria (Chl2A/Chl2B), two Chl*a* molecules (Chl3A and Chl3B) in positions similar to two bacteriopheophytins in the RC of purple bacteria [4,5], and two phylloquinones (A_{1A} and A_{1B}). These electron transfer cofactors are located on two near-symmetric branches, *A* and *B*, corresponding to subunits PsaA and PsaB, respectively. The *A* branch includes Chl1A, Chl2A, Chl3A, and phylloquinone A_{1A}, whereas the *B* branch includes Chl1B, Chl2B, Chl3B, and phylloquinone A_{1B}. The electron transfer chain in PS I therefore includes P_{700}, A_0 (one or both pairs of Chl2A/Chl3A and Chl2B/Chl3B molecules), A_1 (one or both molecules of phylloquinone A_{1A}/A_{1B}), and iron–sulfur clusters F_X, F_A, and F_B. It is now clear that at room temperature, both symmetric branches of cofactors are involved in the electron transfer from P_{700} to F_X [6,7].

In the majority of studies on the fast kinetics of spectral changes in PS I, intense flashes with a duration >100 fs have been used, resulting in the arrival of two quanta at the same RC. Subsequent annihilation of the exciton-induced excitation results in distortion of the spectral changes. In our recent work, we used relatively low power (20 nJ) flashes with a short duration of ~20 fs centered at 720 nm and having a bandwidth of 40 nm (FWHM). This results in preferential excitation of the primary electron donor, the chlorophyll special pair P_{700} [8]. Under these conditions about one-half of the chlorophyll RC molecules (i.e. P_{700} and A_0) are excited directly, whereas the other half receive excitation energy from the antenna chlorophylls (An^*). These conditions were chosen to maximally increase the relative contribution of direct excitation of the RC, which permitted the kinetics of primary stages of the charge separation to be separated from the kinetics of the excitation energy transfer in the antenna. Based on these findings, it was possible to reveal the differential spectra of intermediates $(P_{700}A_0)^*$, $P^+_{700}A^-_0$, and $P^+_{700}A^-_1$, and to describe the kinetics of the transitions between these intermediates. These results can be described by the following scheme:

$$1.\ (P_{700}A_0)^* \xrightarrow{<100\ \text{fs}} P_{700}{}^+A_0{}^- \xrightarrow{\sim 25\ \text{ps}} P_{700}{}^+A_1{}^- \text{ (in ~50\% of the directly excited PS I)}$$

$$2.\ An^* \xrightarrow{\sim 5\ \text{ps}} (P_{700}A_0)^* \xrightarrow{\sim 25\ \text{ps}} P_{700}{}^+A_1{}^- \text{ (in ~50\% of the PS I received excitation from } An^*)$$

Primary charge separation occurs in the femtosecond timescale, making it the fastest event known in any biological system. We have previously observed oscillations of primary charge separation in PS I, apparently caused by coupling with protein vibration modes [9]. Accordingly, the primary charge separation reaction cannot be adequately described within the framework of non-adiabatic Marcus theory [10].

The chlorophylls Chl2A/Chl2B and Chl3A/Chl3B, which comprise the primary electron acceptor A_0, are characterized by unusual axial ligands, i.e. water in the case of Chl2A/Chl2B and Met in the case of Chl3A/Chl3B. The Met ligands to the Chls in the A_{0A} and A_{0B} sites ($Met688_{PsaA}$ and $Met668_{PsaB}$) are conserved in PS I from all known species. In cyanobacteria these ligands have been substituted by Leu, His or Asn [11–13]. Ultrafast optical studies on the A-side variants $M688L_{PsaA}$ and $M688N_{PsaA}$ indicated that forward electron transfer from A_0^- was slowed by a factor of four [12]. In the B-side variants $M668L_{PsaB}$ and $M668N_{PsaB}$, the kinetics of forward electron transfer from A_0^- were similar to the wild type. These data indicate an asymmetric contribution of branches *A* and *B* in secondary charge separation in cyanobacterial PS I. A 95 GHz (W-band) time-resolved EPR study of the $M688N_{PsaA}$ and $M668N_{PsaB}$ variants showed that at 100 K, the EPR observables of $M668N_{PsaB}$ were similar to the wild type, while those of the $M688N_{PsaA}$ variant were distinctly different [14]. An analysis of the out-of-phase echo modulations in the wild type and $M668N_{PsaB}$ variant gave a single population of radical pairs assigned to $P^+_{700}A^-_{1A}$.

The axial ligands to A_0^-, $M688_{PsaA}/M668_{PsaB}$, are positioned midway between A_{0A}/A_{1A}, and between A_{0B}/A_{1B}, respectively. It is therefore possible that the substitution of Met for Asn could influence the properties of either or both A_0 and A_1 by forming a coordination bond with the Mg^{2+} of Chl3A/Chl3B or by forming a H-bond with the C1 carbonyl of phylloquinone.

To study the mechanism of primary events in charge separation, the origin of the asymmetry between cofactor branches, and the possible influence of A_0 axial ligands on the kinetics of electron transfer, a model is needed which connects PS I structure with function. Modern biophysics offers several approaches to molecular modeling, which require various levels of approximation, to connect microscopic information stored in atomic (crystallographic) structure with chemical transitions catalyzed by the protein complex. In contrast to typical chemical systems, protein complexes often consist of up to ~10^5 unique atoms, thus, an adequate microscopic model on the level of Newtonian physics should include ~10^6 degrees of freedom (3 position and 3 velocity coordinates per atom). Modern computers and algorithms have the ability to solve 10^6 Ordinary Different Equations of atomic motion on the microsecond time scale, which was beyond computational limits until recently. However, on the level of quantum physics, the solution of the time-dependent Schrodinger equation even for much smaller atomic systems seems to be unachievable for the next several decades. In response, an integrated approach based on a combination of several approximation levels was developed starting with pioneering work in 1976 [15]. Later, this methodology was applied to the bacterial reaction center (bRC) to study the effect of Tyr (M210) orientation and substitution on the energetics of electron transfer [16]. PS I has a much more complex structure than the bRC, and the details of its function are much more intriguing, as the primary charge separation is the fastest electron transfer reaction in any biological system.

In this work we applied a combined approach to the PS I model that included three central protein subunits together with the corresponding non-protein cofactors (86 chlorophyll molecules, three iron–sulfur clusters, two phylloquinones and 12 molecules of β-carotene) and surrounding water. The description combines three levels of approximation. The primary molecular model (Sections 3.1–3.4) is based on the Newtonian molecular dynamics and explicitly treats complex conformational dynamics of the system coupled to the different charging states of system cofactors. Molecular dynamics (MD) simulations were employed for estimation of structural changes in PS I caused by the primary and secondary electron transfer reactions $(P_{700}A_0) \rightarrow P^+_{700}A^-_0 \rightarrow P^+_{700}A^-_1$. In this model, we considered separately two symmetrical branches of redox active cofactors as possible pathways of electron transfer in native PS I and in two variants, obtained by substitution of two functionally important amino acid residues — the axial ligands of primary electron acceptor ${}_0A_0$ (A_{0A} and A_{0B}). We demonstrated that the explicit molecular dynamics model does not allow an adequate treatment of long-range electrostatic interactions in the system, so we also used (Section 3.4) a complementary semi-continuum (SC) macroscopic approach, proposed in previous studies, which was able to accurately predict the redox potentials of the main electron transfer cofactors in the native complex [17]. However, the macroscopic approach has its limitations in that it cannot reflect the influence of single

amino acid changes, and it required several empirical assumptions for proper application. Additionally, with the aim to improve the treatment of direct chemical interactions of the A_0 axial ligand with two neighboring cofactors (A_0 and A_1), we calculated these interactions in vacuum and in dielectric medium from an ab initio quantum chemical model in the DFT approximation (Section 3.5). With this integrated approach, such fundamental parameters as free energy changes and reorganization energy were calculated, and nonadiabatic semi-classical Marcus theory [10] was used to compare the results of modeling with experimental data.

2. Materials and methods

2.1. Molecular dynamics simulations

Molecular dynamics simulations were conducted for the model based on the crystal 2.5 Å structure of PS I from the cyanobacterium *T. elongatus* (PDB ID: 1JB0) [2]. Its amino acid sequence is over 92% similar with that of *Synechocystis* sp. PCC 6803, which is used in the majority of experimental mutagenic studies of PS I [11–14]. There are only three amino acid residues within 20 Å of A_0 and A_1 that differ between species ($I682_{PsaA}$, $W683_{PsaA}$, and $L684_{PsaB}$ in *T. elongatus* are $V678_{PsaA}$, $F679_{PsaA}$ and $I675_{PsaB}$ in *Synechocystis* sp.), but none of these are in the immediate vicinity of A_0 or A_1. Note that all three changes involve amino acids with similar properties. To reduce the amount of calculations, only three central protein subunits of the complex (PsaA, PsaB and PsaC), together with the corresponding non-protein cofactors (86 chlorophyll molecules, three iron–sulfur clusters, two phylloquinones and 12 molecules of β-carotene), were used for the simulation. The resulting complex was surrounded by water (more than 20,000 molecules) to fill the smallest possible rectangular cell (approx. $140 \times 80 \times 84$ Å); the system as a whole was comprised of approximately 98,000 atoms. Structures of the $M688N_{PsaA}$ and $M668N_{PsaB}$ variants were obtained by single amino acid changes in the SwissPDB program.

Parameterization of atomic interactions for the protein in PS I was based on AMBER molecular potentials [18]. The molecular potentials of chlorophylls, phylloquinones and β-carotenes were derived from potentials computed for similar cofactors in the bacterial photosynthetic RC by ab initio methods [19]. The partial charges of the cofactors in neutral, oxidized and reduced states were derived by Mulliken population analysis using the density functional approximation PBE0 [20,21] in the GAMESS program [22]. Parameterization of the iron–sulfur clusters [Fe_4S_4 (SCH_3)$_4$] was based on [23].

Molecular dynamics simulations were conducted using the NAMD 2.7 program [24] on the "Chebyshev" supercomputer in the Moscow State University Computing Centre. The molecular dynamics simulation step was 1 fs. A constant pressure of 1 atm was maintained at all stages of the simulation; the temperature was kept at 298 K; the volume of the system was changed independently and without restriction in all dimensions by the Nose–Hoover Langevin piston method. In all cases, a three-step preparatory sequence was carried out: energy minimization of the entire system using the internal NAMD gradient descent algorithm, 10,000 steps; molecular dynamics with harmonic constraints on the positions of water oxygen atoms for 500 ps (500,000 steps, the force constant of harmonic potential decreased from 1 to 0.1 kcal/mol·Å); and molecular dynamics for 5 ns without restrictions. The final coordinates of the system atoms were used as an initial state for simulations of electron transfer. In this study, it was assumed that electron transfer occurs in two stages, with the formation of the following configurations of charged cofactors (chlorophyll special pair P_{700}, chlorophyll A_0 and phylloquinone A_1):

- a neutral state ($P_{700}A_0A_1$, state N);
- primary radical pair ($P_{700}^{+}A_0^{-}A_1$, state A_0^{-});
- secondary radical pair ($P_{700}^{+}A_0A_1^{-}$, state A_1^{-}).

We considered primary electron donor P_{700} as dimer of chlorophylls Chl1A and Chl1B and A_0 as a monomeric chlorophyll Chl3A/Chl3B, i.e. not including Chl2A/Chl2B. For each of the three systems (wild type and the two variants), charge transfer along either cofactor chains *A* or *B* was simulated independently, which resulted in six independent series of simulations; when simulating the charged state of the chlorophyll special pair P_{700}, only one chlorophyll molecule (in the corresponding chain) was charged.

All systems were simulated successively in the three charged states (the last frame of the trajectory in one charged state was used as the initial condition for subsequent modeling in the subsequent charged state) in two series: long-term (5 ns) simulations, with atomic coordinates recorded every 10 ps, and short-term (100 ps) simulations, with atomic coordinates recorded every 1 ps. The latter series was repeated 40 to 50 times, with frames from the second half of the corresponding 5 ns trajectory with an interval of 50 ps taken as the initial conformations.

The results of molecular dynamics simulations were studied using the VMD program [25]. The primary analysis of trajectory files (retrieval of atomic coordinates in explicit form) was carried out in MATLAB using scripts from the MatDCD package of MDTools suite developed by the Theoretical and Computational Biophysics group at the Beckman Institute, University of Illinois. Calculations of outer sphere reorganization energy, changes in cofactors relative positions, etc. were performed in MATLAB.

2.2. Semi-continuum macroscopic model

The results obtained by MD were compared with a semi-continuum (SC) macroscopic model developed earlier in [17]. The electrostatic field was calculated by using the program DelPhi (DelPhi V. 4 Release 1.0), which allows the simultaneous treatment of several dielectric regions [26]. The numerical solution of the Poisson–Boltzmann equation was carried out in a three-dimensional grid with a space interval of 1.0 Å and margins of 30 Å to 50 Å. The protein was considered as a heterogeneous dielectric medium, and the static dielectric permittivity distribution $\varepsilon(prot)_s$ was taken as in [17]. The optical dielectric constant for protein was taken as $\varepsilon(prot)_o = 2.5$ [27]. The surrounding water was considered as a dielectric medium with static and optical dielectric constants $\varepsilon(wat)_s = 81$ and $\varepsilon(wat)_o = 1.8$, correspondingly. The reorganization energy of the primary and secondary charge transfer reactions was calculated as a change of Born energy of the donor–acceptor electric dipole transferred from the static dielectric medium into the optical environment. This approach generalizes the Marcus approach [10] to heterogeneous dielectric media.

2.3. Quantum chemistry calculations

The Firefly QC package [28], which is partially based on the GAMESS (US) [22] source code, was used to compute ground-state energies of (cofactor + ligand residue) structures of wild type and variant PS I in neutral and charged forms. Atom coordinates were taken from the X-ray crystal structure (PDB ID: 1JB0) in the case of wild type PS I, and from an averaged structure of a 5 ns molecular dynamics trajectory in the case of the Met→Asn substitution. H-atom coordinates were adjusted by DFT geometry optimization. To simplify the calculations, the hydrocarbon chains of chlorophyll and phylloquinone, as well as several aliphatic side-groups of chlorophyll not contributing to the π-electron system, were cut off (see Fig. 3). To study the impact of Asn rotation on cofactor redox potentials, 36 systems with different positions of the Asn terminal $CONH_2$ group were generated, with a step of 10°.

DFT calculations with the modified hybrid functional of Perdew, Burke and Ernzerh (PBE0) were carried out [20,21]. Calculations were initially performed in the minimal basis 6-31G and then refined in the basis 6-311G with added diffuse *sp* orbitals [29]. Energies were calculated individually for A_0 and A_1 with the ligand (Met or Asn); initial molecular orbitals for charged cofactor states were taken from those obtained

for neutral states. The changes in the cofactor redox potential caused by the Met➔Asn substitution were calculated as the double energy difference between the charged and neutral states: $\Delta E = (E_{red}(Asn) - E_{ox}(Asn)) - (E_{red}(Met) - E_{ox}(Met))$, where the model system comprises cofactor (A_0 or A_1) and ligand (Met or Asn) in the neutral (oxidized, ox.) and charged (reduced, red.) states.

2.4. Reorganization energy calculations

The electron transfer rate constant (k_{et}) was approximated by the Marcus equation for electron tunneling [10]:

$$k_{et} = \frac{2\pi|V|^2}{\sqrt{4\pi\lambda k_B T}} e^{-\frac{(\lambda+\Delta G^0)^2}{4\lambda k_B T}}, \quad (1)$$

where V is the electronic coupling matrix element, which depends on the distance between the reactants, ΔG^0 is the reaction free energy change, k_B is the Boltzmann constant, T is the temperature, and λ is the reorganization energy of reaction, which can be split into the reorganization energy of medium (λ_{out}, the outer sphere part) and reactants (λ_{in}, the inner sphere part). The value of λ_{in} for porphyrin-based cofactors was estimated to be in the range of 100-150 meV [30,31]. The values of λ_{out} were obtained directly from MD simulations as one half of the electric potential difference of the donor and the acceptor. The charge distributions for different donor/acceptor states were taken from the DFT calculations described in Section 2.3.

The dependence of electron transfer rate on the edge-to-edge distance R between cofactors was estimated according to the Moser–Dutton empirical approximation [32]:

$$\log k_{et} = 15.16 - 0.6R - 3.1\left(\Delta G^0 + \lambda\right)^2/\lambda \quad (2)$$

3. Results and discussion

3.1. Molecular dynamics model of PS I

An MD model of PS I from the cyanobacterium *T. elongatus* was built based on the 2.5 Å X-ray crystal structure (PDB ID: 1JB0). Only the three central subunits crucial to its function were included in the simulation to lessen the required computations. The dimensions of the simulation cell were 140 × 80 × 84 Å; the PS I complex was surrounded by water to fill the smallest possible cell due to computational limits, which resulted in a rather thin (~5 Å) water buffer along regions where the protein was closest to the simulation cell border. The structure consisted of ~24,000 atoms of protein, ~13,000 atoms of cofactors (mainly chlorophylls) and ~20,000 molecules of water. Thermal atom fluctuations around equilibrium positions, as measured by RMSD calculations in a variable 200 ps window along 15-ns trajectory, were ~0.5 Å.

To estimate the possible influence of the distance between the redox cofactors on the electron transfer rate and to assess the overall stability of the system, the distances between P_{700}, A_0 and A_1 were measured using 5 ns simulations of wild-type and variant PS I in different charged states. The distance was measured between atoms comprising conjugated electron systems of cofactors (chlorophylls and quinones): the distance of primary electron transfer was measured between Chl1A/Chl1B and Chl3A/Chl3B, and the distance of secondary electron transfer was measured between Chl3A/Chl3B and A_{1A}/A_{1B}. The system was found to be quite stable: the standard deviations of distances between the cofactors were less than 0.1 Å both in the wild-type and in the variants, and were independent of charge state. The distance of primary electron transfer in all structures was found to be 12.4 Å and 14.4 Å in the branches *A* and *B*, respectively. The distance of secondary electron transfer was 7.1 Å in branch *A* and 6.6 Å in branch *B*.

In accordance with the empirical Eq. (2), the small shifts in the geometry caused by the Met to Asn substitution could not be responsible for the changes in charge separation rates observed experimentally [12]. Additionally, the differences in cofactor arrangement in branches *A* and *B* are too small to explain the asymmetry of electron transfer. For this reason we analyzed dynamic and energetic microscopic characteristics of dielectric polarization processes coupled with the electron transfer reactions separately in branches *A* and *B* of the wild type and the variants.

3.2. Structural flexibility of wild-type and variant PS I

To study structural movements in PS I, we obtained average structures by superimposing individual frames of 5 ns simulations. To exclude slow diffusion movements, we superimposed the positions of the C_α-atoms in each frame over their positions in the first frame. The local protein flexibility was calculated as mean C_α-atom deviations from their average positions. The resulting map of flexibility for the wild-type PS I is shown in Fig. 1.

It was found that PS I has a relatively rigid hydrophobic core despite the absence of several subunits and a surrounding water environment instead of membrane. The protein flexibility was rather heterogeneous, splitting into several apparent layers with different flexibilities distributed along the normal to the membrane plane. This layered structure corresponds to the previously described PS I dielectric heterogeneity [17].

To characterize the dynamic response of PS I to cofactor charging, we analyzed atom shifts in the neighborhood of P_{700}, A_0 and A_1 caused by the primary and secondary charge separation reactions. As these processes in PS I occur within 100 ps, we analyzed a series of short 100 ps molecular dynamics trajectories with independent starting conformations. A total of 40 initial conformations were taken from 5 ns molecular dynamics simulation in the N-state; the final frame of the 100 ps N-state trajectory was used as the starting conformation for the A_0-state trajectory, and the final frame of 100 ps A_0-state trajectory was used as the starting point for the A_1-state trajectory. This procedure was repeated for the wild type and variants of PS I with the charge separation occurring through either the *A* or the *B* branch of cofactors.

Average conformations were obtained individually for the second half of each trajectory in the set, yielding 40 groups of three structures in consecutively charge states. For the description of the response to electron transfer, the averaged atom coordinates in the N-state were subtracted from the coordinates in the A_1^- state, and the obtained atom shifts were averaged through the 40 sets of independent trajectories. In this work we made an attempt to discover differences in flexibility of PS I along the *A* and *B* branches that may underlie the experimentally observed asymmetry in electron transfer along these branches of electron cofactors [11–14]. Only atoms in a 10 Å neighborhood from the chlorophyll special pair P_{700} and phylloquinone A_1 in both chains (excluding the alkyl tails) with magnitudes >0.5 Å were taken into account. This procedure was repeated for both variants of PS I, separately for the electron transfer in the two cofactor branches.

Comparing the protein response to electron transfer in branches *A* and *B* of the wild type, we found that atom shifts in branch *B* caused by two consequent electron transfer reactions were ~1.5 times more numerous than in branch *A*, which indicates a greater mobility of the protein in the vicinity of branch *B* (Fig. 2A). To reveal the features that control the experimentally observed asymmetry in electron transfer along the different branches, the involvement of individual asymmetrical amino acids in the energetics of electron transfer reactions should be investigated, which is described in Sections 3.3, 3.4 and 3.5. Similar results were obtained for the $M688N_{PsaA}$ and $M668N_{PsaB}$ variants. Comparing the variants with wild type PS I, the replacement of Met by Asn in either of the branches induced additional atom shifts in response to charge separation, an effect observed even in the opposing protein

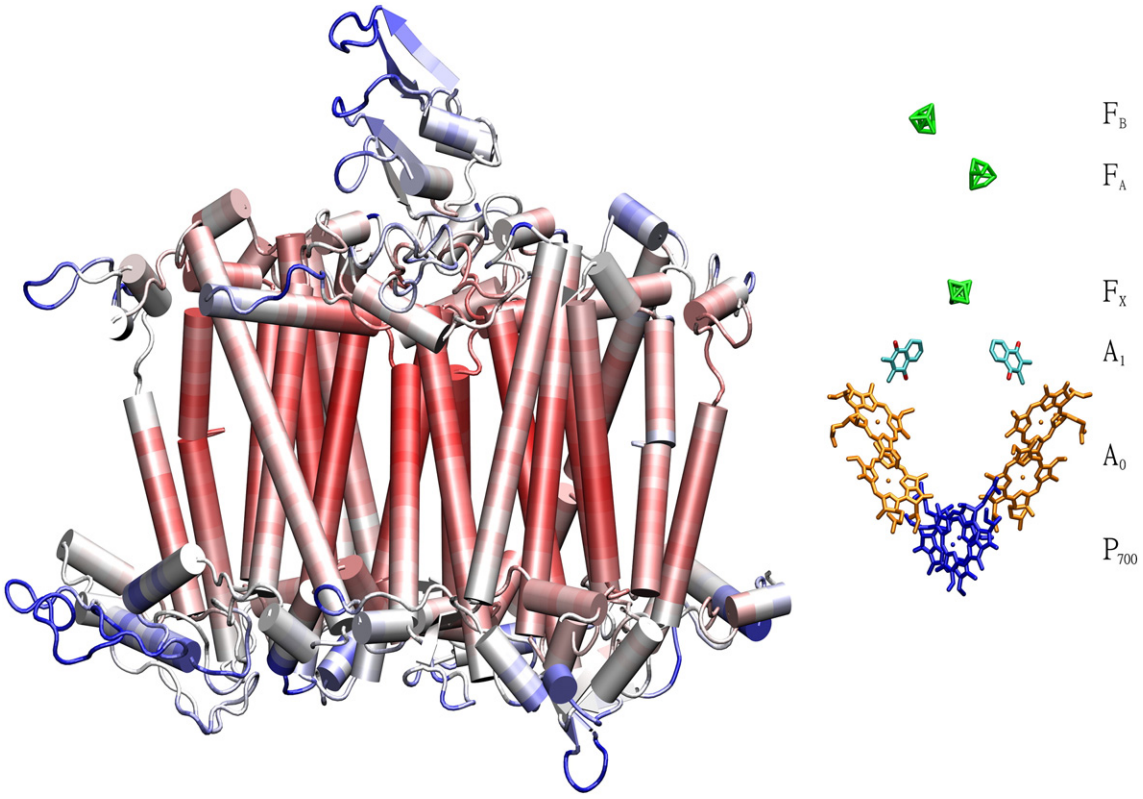

Fig. 1. Structural flexibility map of PS I. Color indicates spatial mobility of amino acids, from red (most rigid) to blue (most mobile). α-Helices and β-sheets are shown schematically.

chain (Fig. 2B, C), which significantly affects the reorganization energy of electron transfer, as will be shown in Section 3.4.

The quantitative analysis of the response of the protein to electron transfer events in both branches of cofactors as well as the effects of Met to Asn substitutions are described further in Section 3.4 in which the results of MD simulations are compared with the SC macroscopic model.

3.3. Conformational changes of the chlorophyll A_0 axial ligand in wild type and variant PS I

The immediate environment of the electron transfer cofactors can influence their properties, as demonstrated by the significant differences in the redox potentials of similar cofactors in PS I. In the previous section, general qualitative characteristics of protein motion in the vicinity of the electron transfer cofactors were taken into consideration. In this section, we analyze in detail the conformational dynamics of the axial ligand of chlorophyll A_0 (Met and Asn), because only this residue was found to be changing its rotamer conformation after the primary charge separation reaction in the PS I variants. A similar effect of Tyr (M210) rotation on the energetics of electron transfer in the bRC was studied earlier by PDLD/MD simulations [16].

The dynamics of the immediate environment of chlorophyll A_0 (Chl3) in wild-type and variant PS I were studied using 5 ns MD trajectories. In wild-type PS I, the Chl3A/Chl3B magnesium atom forms a Van der Waals bond with the sulfur atom of methionine, the conformation of which is stable (Figs. 3A, 4A), while the oxygen atom attached to C1 of phylloquinone A_1 does not have a definite ligand. In PS I from the variant strains, the chlorophyll A_0 ligand position is occupied by the carbonyl oxygen of the asparagine side chain in the neutral state of A_0 (Fig. 3B). MD showed that this conformation of asparagine is relatively stable at least for 5 ns in the neutral state of the cofactors. However, the appearance of a negative charge on the porphyrin ring Chl3A/Chl3B (state A_0^-) destabilizes this conformation, and the amide group of asparagine may lose its hydrogen bond with the carbonyl oxygen of phylloquinone A_1 with a characteristic time of less than 1 ns. Simultaneously, the bond between the oxygen atom of asparagine and the magnesium atom of chlorophyll A_0 Chl3A/Chl3B breaks, and the entire group rotates toward the porphyrin ring of chlorophyll A_0 Chl3A/Chl3B, forming a new hydrogen bond between the Chl3A/Chl3B magnesium atom and the oxygen atom of asparagine (Fig. 3C).

This rotation occurs along χ_2 torsion angle, which is formed by the planes of the C_α–C_β–C_γ atoms and the C_β–C_γ–S_δ atoms for methionine or the C_β–C_γ–N_δ atoms for asparagine. Simulation trajectories of wild-type and variant PS I in different charge separation states (N, A_0^- and A_1^-) in the nanosecond scale were used to collect statistical information on the χ_2 angle of the A_0 ligand (Fig. 4A, variant $M668N_{PsaB}$ not shown). The N state and A_1^- state were analyzed on 5 ns long trajectories, whereas the calculation time for the A_0^- state was increased to 20 ns to study the observed rotations of Asn in $M688N_{PsaA}$ and $M668N_{PsaB}$ variants. It was demonstrated that χ_2 distributions for the variants differ from each other: the side chain of asparagine in state A_0^- rotates in different directions, namely counter-clockwise in the case of $M688N_{PsaA}$ and clockwise in the case of $M668N_{PsaB}$ (Fig. 4B). This is an indication of asymmetry in the protein environment of the chlorophyll Chl3A/Chl3B axial ligand in chains *A* and *B*.

The full set of rotational dynamics of the axial ligand of chlorophyll A_0 in the $M668N_{PsaB}$ variant is shown in Fig. S1 (Supplementary material). We observed a wide angle distribution of the Asn residue in $M688N_{PsaA}$/$M668N_{PsaB}$ variants in the A_0^- redox state, where it was possible to distinguish two distinct rotamer conformations. The rate of such conformational changes is predicted to be very sensitive to the details of the molecular parameters used to model the interactions between Asn and chlorophyll in its anionic state (A_0^-) and the neutral phylloquinone (A_1). Due to complex nature of such interactions (which include specific quantum effects of electron correlations in the porphyrin ring of anionic chlorophyll, Asn–Mg coordination, hydrogen bonding effects, effects of protein environment), we could not consider them with the

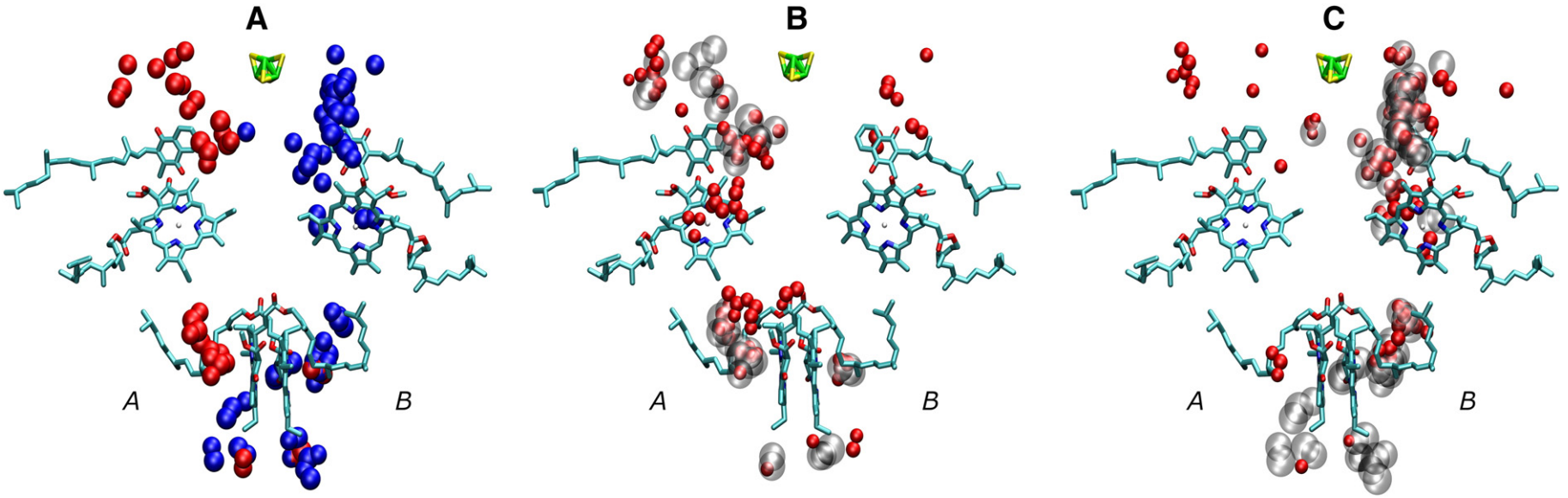

Fig. 2. Atom shifts in PS I induced by cofactor charging. Atoms of polar amino acids within 10 Å from P_{700}, A_{1A} and A_{1B} and moved >0.1 Å in response to the charge separation reactions ($N \rightarrow A_1^-$) are shown. Cofactors of electron transfer (P_{700}, A_0, A_1, iron–sulfur cluster F_X) are shown in cyan. (A) Atom shifts in wild type PS I in response to cofactor charging in branches *A* (red spheres) and *B* (blue spheres). (B) Atom shifts in response to the cofactor charging in branch *A* in the wild type (gray transparent spheres) and the $M688N_{PsaA}$ variant (red opaque spheres). (C) Atom shifts in response to cofactor charging in branch *B* in the wild type (gray transparent spheres) and the $M668N_{PsaB}$ mutant (red opaque spheres).

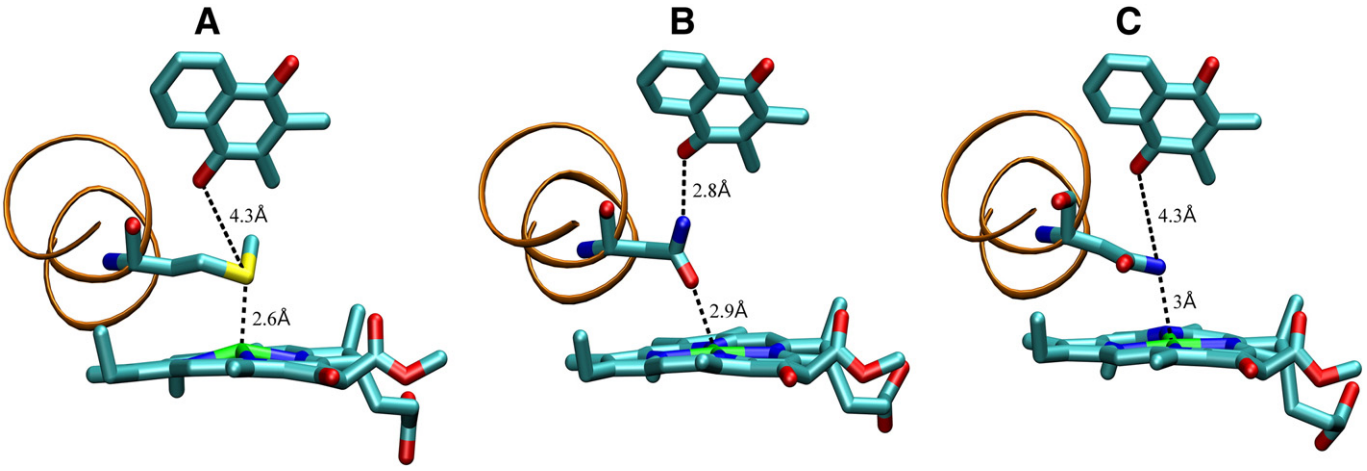

Fig. 3. Conformations of chlorophyll A_0 axial ligand, $Met688_{PsaA}$ in the wild type (A) or $Asn688_{PsaA}$ in the variant (B, C). The α-helix bearing the A_0 axial ligand is shown as an orange ribbon. Wild type conformation (A) was taken from the crystallographic structure. Conformations of $Asn688_{PsaA}$ taken from MD simulation of the variant demonstrate the most probable position in the N and A_1^- states (B), and the alternative rotated position in the A_0^- state (C).

appropriate level of accuracy using the MD method. For this reason, the quantitative estimations in Sections 3.4 and 3.5 within the framework of the integrated MD/SC/QC approach represent only the first, preliminary attempt of such an analysis.

3.4. Dielectric response and reorganization energy of the charge separation reactions

In this section, quantitative characteristics of the response of protein to charge separation in wild type and variant PS I are calculated in both branches using the sets of 100 ps trajectories described in Section 3.2. The electrostatic potential on each of the main cofactors (chlorophyll special pair P_{700}, chlorophyll A_0, phylloquinone A_1) was calculated directly from MD trajectories using the partial atomic charges described in Materials and methods. To eliminate artifacts caused by slow movements, the potential values were calculated separately for each pair in the 40 sets of consequent 100 ps trajectories and the obtained differences were averaged. The reorganization energy of the reaction was calculated as one half of the electrostatic energy

$$\lambda = \frac{1}{2}\sum_i \delta q_i \cdot \Delta\varphi_i, \tag{3}$$

where δq_i is the change of partial electric charge at atom *i* of the charging cofactor and $\Delta\varphi_i$ is the change of electric potential at atom *i* caused by the dielectric response of the cofactor environment (the reaction field). The calculation errors were estimated as standard errors of the mean. It is convenient to split the potential change into three parts: the contribution from protein (including non-charging cofactors), bound water, and bulk water. These contributions and the total reorganization energy are given in Table 1.

The reorganization energy of primary charge separation λ_1 calculated by MD was approximately the same, with a value of ~390 mV, for both branches of wild-type PS I. The reorganization energy of this reaction

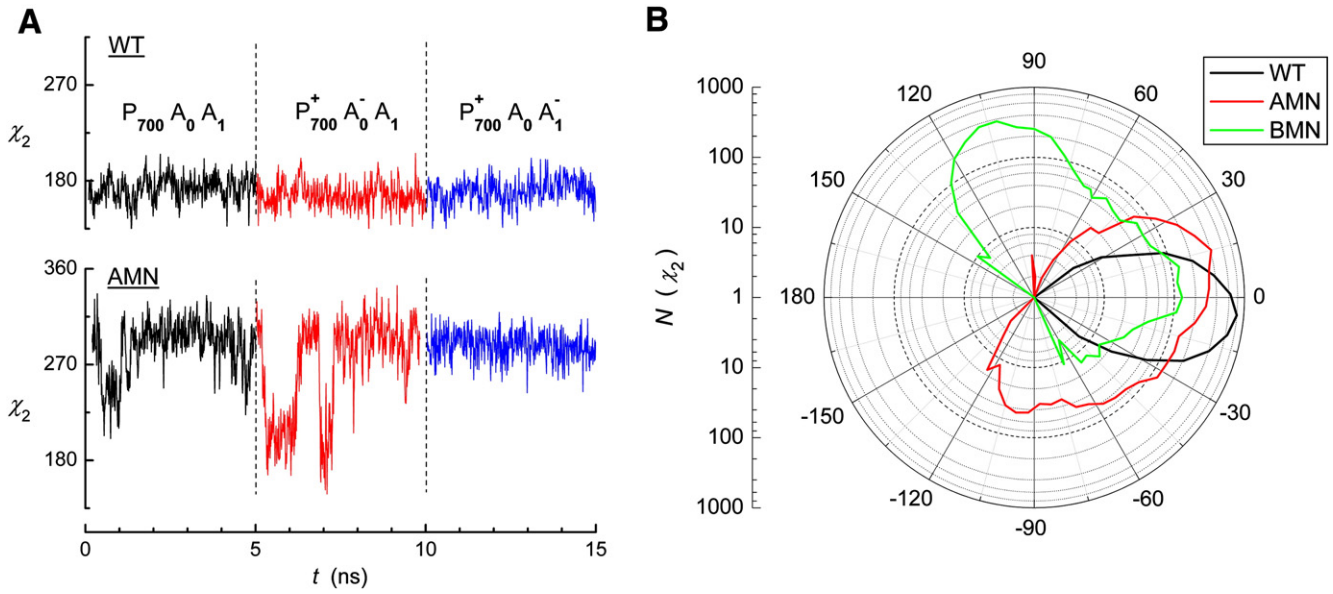

Fig. 4. Rotation of the side chain of the chlorophyll A_0 axial ligand. (A) Torsion angles χ_2 in the wild type (top) and the $A688MN_{PsaA}$ variant (bottom) were obtained from 5 ns MD trajectories in consecutive charge states: N (black), A_0^- (red) and A_1^- (blue). (B) Histogram of chlorophyll A_0 axial ligand position in PS I of the wild type (black), the $M688N_{PsaA}$ variant (red) and the $M668N_{PsaB}$ variant (green) in the A_0^- state. Logarithmic scale; mean residue position in the N state was chosen as zero angle.

for the modified cofactors of variant PS I was found to be 30 to 40 meV higher, which is similar to the results of the wild-type considering calculation error, whereas the kinetics of primary electron transfer through the unmodified cofactors of variant PS I were identical to the wild type. However, there is quite a significant difference between the reorganization energies λ_2 of secondary charge separation between the wild-type (445 and 480 meV for branches *A* and *B*, respectively) and the variants (585 and 590 meV). These differences exceed the calculation error by more than twofold, and therefore can be considered significant.

The reorganization energies of the same reactions in wild type PS I were calculated by the alternative SC approach, described by Ptushenko et al. [17], based on the X-ray crystal structure. The reorganization energies of primary charge separation (330 meV for electron transfer through either branch) were found to be 60 meV lower than obtained by the MD method. However, the secondary charge separation was characterized by a much lower reorganization energy of 230 meV.

Note that the number of bulk water molecules added to the protein structure in the MD simulation was limited by the available computing power, and for the calculations of the reorganization energy of electron transfer reactions this was insufficient to describe properly the influence of the aqueous medium. The contribution of this bulk water was estimated by the SC macroscopic model and found to be only ~30 meV for the first charge separation reaction and ~20 meV for the second charge separation reaction (see Table 1). However, there exists a population of water molecules tightly bound to the protein matrix whose contribution to the reorganization energy should be calculated directly. To discriminate these tightly bound water molecules, a 15 ns long molecular dynamics simulation was examined for water molecules that moved less than 5 Å relative to the protein matrix in 5 ns. Out of approximately 20,000 water molecules in the simulation cell, about 300 met this criterion. These water molecules were therefore excluded from the macroscopic calculations and their effect on the electric potentials of the cofactors and their reorganization energy was calculated directly. The orientation of most of these molecules was quite stable, and their contributions to the reorganization energy of the primary and secondary charge separations were found to be less than 60 meV. In previous SC studies of redox potentials of the PS I cofactors [17] we had to manually set the orientation of 20 molecules of water that are tightly bound in closed pockets near the F_X iron–sulfur cluster and therefore cannot be accessed as part of the water continuum. MD methods eliminate the inconsistency of such an empirical approach. These internal water clusters are oriented in such a way that their electrostatic contribution is positive for the phylloquinone in branch *A* and negative for the phylloquinone in branch *B*. The asymmetry in the orientations of these molecules may, in part, be responsible for the observed asymmetry of the redox potentials of Q_A (A_{1A}) and Q_B (A_{1B}).

We tried to estimate the redox potentials of the cofactors using the MD method and we calculated the electric potential on the cofactors generated by electric charges of the entire system. However, the absolute values of these potentials were found to be greatly affected by distantly changed amino acid residues. The electrostatic field of these distantly charged residues should be largely screened by the bulk water. However, due to computational limitations we were able to simulate only a thin layer of water around the protein, which was insufficient to properly represent the water continuum. Due to this limitation, the long-range effects of these residues contribute significantly to the total electric potentials on the PS I cofactors. These effects resulted in very high absolute potentials on the cofactors, in the range of volts, and in unrealistic absolute differences between the potentials of different cofactors. At the same time, as these amino acid residues are very distant from the reaction center core, the contribution of these residues to the reorganization energy of charge separation was found to be insignificant.

Thus, MD simulations provide a powerful tool to analyze quantitatively the protein reorganization at moderate distances from the reaction center in response to cofactor charging during electron transfer reactions, but this approach fails in calculations of absolute electric potential values due to the long-range character of electrostatic interactions. To the contrary, the SC macroscopic approach has difficulties in the treatment of local dielectric heterogeneity of the protein, but it succeeds in the analysis of long-range interactions. Both approaches are mutually complementary. However, both methods lack the capability to analyze direct chemical effects of ligand–cofactor interactions, which can be obtained from quantum chemistry methods.

If secondary electron transfer in PS I is independent of temperature, we may assume that in wild-type PS I the reorganization energy of this reaction matches the free energy gap ($\lambda_2 = -\Delta G_2$). Taking the obtained value of outer-sphere reorganization energy from Table 1 and the ΔG_2 value for secondary electron transfer as the difference of the A_0 and A_1 redox potentials in branch *A*, we estimate the inner-sphere reorganization energy of secondary electron transfer to be ~115 mV, which is close to the reorganization energy of porphyrin reduction in vacuum [30,31]. According to the Moser–Dutton Eq. (2), the increase of λ_2 by ~150 meV due to the Met to Asn substitution could decrease the reaction rate by 20 to 50%, whereas the experimental data suggest a slowdown of 3 to 5 fold. To investigate the possible reasons for such a large deceleration we employed quantum chemistry calculations to study the direct interactions of A_0 and A_1 in the asparagine variants.

MD calculations allow one to estimate the contributions of individual amino acids to the total reorganization energy according to Eq. (3). It was found that the major part of the outer sphere reorganization energy can be attributed to a very small number of amino acids, with 15 to 20 residues comprising over 50% of the total value in the case of primary electron transfer. Secondary electron transfer, which occurs over a much shorter distance, is affected by its immediate environment even more strongly, with 10 and 5 residues in chains *A* and *B*, respectively, contributing 60% to the total reorganization energy of electron transfer in the corresponding branch. In a comparison of wild type and variant

Table 1
Outer-sphere reorganization energy of primary and secondary electron transfers in PS I of wild type and variants, estimated on a series of 100 ps molecular dynamics (MD) simulations or by semi-continuum (SC) model. Contributions of protein, protein-bound water and bulk water are shown. The inner sphere reorganization energy of A_0 and A_1 during the secondary electron transfer was taken as 110 meV in all cases [30,31].

Active cofactor branch	System type		Primary charge separation λ_{out}, meV				Secondary charge separation λ_{out}, meV			
			Protein	Water		Total	Protein	Water		Total
				Inner	Bulk			Inner	Bulk	
A	Wild-type	MD	335 ± 20	55		390 ± 20	380 ± 15	65		445 ± 15
		SC			<33	330 ± 20			<20	230 ± 20
	$M688N_{PsaA}$		370 ± 20	50		420 ± 20	530 ± 35	55		585 ± 35
	$M668N_{PsaB}$		345 ± 20	45		390 ± 20	390 ± 20	60		450 ± 20
B	Wild-type	MD	375 ± 20	20		395 ± 20	430 ± 20	50		480 ± 20
		SC			<33	330 ± 20			<20	230 ± 20
	$M688N_{PsaA}$		370 ± 20	25		395 ± 20	420 ± 20	55		475 ± 20
	$M668N_{PsaB}$		400 ± 20	35		435 ± 20	540 ± 20	50		590 ± 20

PS I, it is shown that the significant part of the difference in outer sphere reorganization energy can be attributed to the altered residue alone. In the $M688N_{PsaA}$ variant the contribution of $Asn688_{PsaA}$ increased by 70 mV as compared to Met688 of the wild type, whereas in $M668N_{PsaB}$ variant, the contribution of the ligand to Chl3B increased by 100 mV. Other notable residues, whose contributions to the reorganization energy of the secondary charge separation reactions were larger than 30 mV, included $Asp473_{PsaA}$, $Ser692_{PsaA}$, and $Leu722_{PsaA}$ in the case of the $M688N_{PsaA}$ variant and $Thr665_{PsaB}$, $Ser672_{PsaB}$, $Arg674_{PsaB}$ and $Trp677_{PsaB}$ in the case of the $M668N_{PsaB}$ variant. These results may explain the ~200 mV difference between the estimations of secondary electron transfer reorganization energies obtained by the MD and SC approaches. Significant movements of the amino acids in the immediate vicinity of A_0 and A_1 induced by electron transfer greatly affect the reorganization energy of this reaction, but are not taken into account by the SC approach.

The accuracy of our MD/SC estimations depends on several factors. Some of these factors could be considered within the molecular mechanics approach itself. In particular, we show that the restricted size of our MD system does not introduce a significant error into the calculations of the reorganization energy of the charge separation reactions in the protein core (see above), and that the inaccuracy could be counterbalanced within the SC approach. Another source of error is an insufficient time of MD simulations for an adequate configuration space sampling. In fact, within the MD approach itself there are some methods for acceleration of such sampling. In our system the rotation of Asn in the A_0^- redox state between the two rotamer conformations occurs with a characteristic time of ~1 ns, hence, an appropriate configuration sampling would require at least 100 ns long simulations. Because the distributions in Fig. 4 were obtained from 20 ns long trajectories, they can only be considered as qualitative estimates. However, the experimental data reveal that the lifetime of the A_0^- redox state in Met-substituted PS I variants is ~100 ps [12], and we do not expect a complete relaxation of the Asn residue in response to the primary charge separation reaction. To partially counteract the sampling problem we analyzed sets of ~40 independent 100 ps trajectories and obtained respective free energy changes by averaging the obtained values. Statistical analysis of the results gives a value of the respective error less than 30 meV, which is satisfactory for our purposes.

Other types of errors could not be analyzed within the MD/SC approach because they are caused by the restrictions of the molecular mechanics model itself. To improve the accuracy of MD/SC approach, we treat the direct interaction of the axial ligand with A_0 and A_1 by the methods of quantum chemistry in Section 3.5.

3.5. Quantum effects of the axial Chl3 ligand on the redox potentials of A_0 and A_1

A large conformational motion of $Asn688_{PsaA}$/$Asn668_{PsaB}$ in the direct vicinity of A_0 and A_1 could significantly alter the redox potential of both cofactors and require more accurate consideration than is possible in the MD approach. In the framework of MD simulations, we observed that the rotation of $Asn688_{PsaA}$/$Asn668_{PsaB}$ along the C_β–C_γ bond (χ_2 torsion angle, see Section 3.3) is tightly correlated with the difference between the electrostatic potentials at A_0 and A_1, which in turn is related to λ_2 (Fig. 5). As shown in Figs. 4 and 5, $Asn688_{PsaA}$/$Asn668_{PsaB}$ in the A_0^- state adopts two relatively stable conformations, "non-rotated" and "rotated" by approximately $\pm 110°$. The transition between these conformations increases the potential at A_0 by ~100 mV (not shown) and decreases the potential at A_1 by ~260 mV (Fig. 5). The total effect of ~360 mV corresponds to the maximal contribution of the Asn rotation to the reorganization energy of secondary electron transfer as much as ~180 meV. This MD modeling takes into account the Coulomb effect of Asn rotation on A_0/A_1 and the respective dielectric screening by a polar environment (atomic and orientational polarization of protein and solvent), but does not include direct chemical interactions (ligand-Mg coordination in the chlorophyll ring, hydrogen bonding and electron correlation effects). The chemical effects could be assessed by methods of quantum chemistry, but the latter are hardly applicable to an accurate configuration sampling done within the MD approach.

Therefore, we developed an integrated approach, which is based on a combination of the results of MD simulations and their refinement by ab initio DFT calculations. We aimed to separate the contribution of the Asn residue from the general effect of protein environment; the latter was taken solely from the results of MD modeling, whereas the former was initially obtained from MD results and then refined by QC methods.

We used the DFT approximation for ab initio estimation of energy changes caused by the Asn rotation along the C_β–C_γ bond (χ_2 torsion angle), which could be considered as a reaction coordinate tightly correlated with the electrostatic potential changes (Fig. 5). Namely, the ground-state energies of chlorophyll A_0 in the neutral and anionic states, $E_{0ox}(\chi_2)$ and $E_{0red}(\chi_2)$, and of phylloquinone A_1, $E_{1ox}(\chi_2)$ and $E_{1red}(\chi_2)$, were calculated with either Met or Asn residue. The calculations were done in vacuum and did not take into account other chemical groups, and in addition, we estimated the effect of a polar dielectric environment on the redox potential of the chlorophyll–ligand complex. The geometry of cofactors was obtained by energy minimization with constraints imposed on the conformation of chlorophyll, phylloquinone and Met/Asn to preserve the crystallographic structure. All internal coordinates of the system were then fixed except for the torsion angle χ_2, which was rotated from 0 to 350° with steps of 10°, resulting in 36 different conformations, and the energy differences, $E_{0red}(\chi_2) - E_{0ox}(\chi_2)$ and $E_{1red}(\chi_2) - E_{1ox}(\chi_2)$, between the anionic and neutral states of cofactors A_0 and A_1 for variant PS I complexes were calculated. For comparison of these data with the respective redox potentials in wild type PS I, we subtracted from them the energy differences $E_{0red}(WT) - E_{0ox}(WT)$ and $E_{1red}(WT) - E_{1ox}(WT)$ of A_0 and A_1 with Met in the wild type conformation (which was stable and did not change in different redox states, as seen in Fig. 4). The resulting double differences $\Delta E_0 = (E_{0red}(\chi_2) - E_{0ox}(\chi_2)) - (E_{0red}(WT) - E_{0ox}(WT))$ and $\Delta E_1 = (E_{1red}(\chi_2) - E_{1ox}(\chi_2)) - (E_{1red}(WT) - E_{1ox}(WT))$ are plotted in Fig. 6. The zero angle χ_2 in Fig. 6 corresponds to the conformation of Asn in the neutral state (the peak at zero angle in Fig. 4B). Position of the blue arrows in Fig. 6 indicates the Asn rotation angle in the neutral state of PS I, and position of the red arrows indicates the rotated Asn conformation in the A_0^- state of the $M688N_{PsaA}$ variant. Filled arrows correspond to redox potential shifts of A_0, and open arrows correspond to redox potential shifts of A_1.

The energy profiles in Fig. 6 demonstrate that the substitution of Met by Asn alters substantially the redox potentials of the PS I cofactors. Firstly, in the basic conformation of Asn in the neutral state ($\chi_2 = 0$), the redox potential of A_0 is lower by ~90 mV compared to the wild type, apparently due to the effect of the oxygen atom of Asn bonded to the magnesium atom of the chlorophyll (the positive energy shift indicated by the open blue arrows in Figs. 6 and 7). The rotation of Asn to its position ($\chi_2 = -100°/\chi_2 = +110°$) observed in long 5 ns simulations raises the redox potential of A_0 by ~350 mV, which decreases the energy of the A_0^- state by ~250 meV relative to the wild type (the red filled arrows in Figs. 6 and 7).

Therefore, if the driving force of the primary charge separation is less than 90 meV, electron transfer should be coupled with Asn rotation. Alternatively, if the difference of energies between $(P_{700}A_0)^*$ and $P_{700}^+A_0^-$ states is larger than 90 meV, primary charge separation might occur independent of the Asn position, but the Asn rotation may still happen during the lifetime of the A_0^- state, as shown by the results of MD simulations. In any case, the Met to Asn substitution would slow down primary charge separation, but because ultrafast electron transfer reactions that occur in the femtosecond time scale cannot be treated in the framework of the nonadiabatic semiclassical approximation (1), we could not consider these effects more quantitatively.

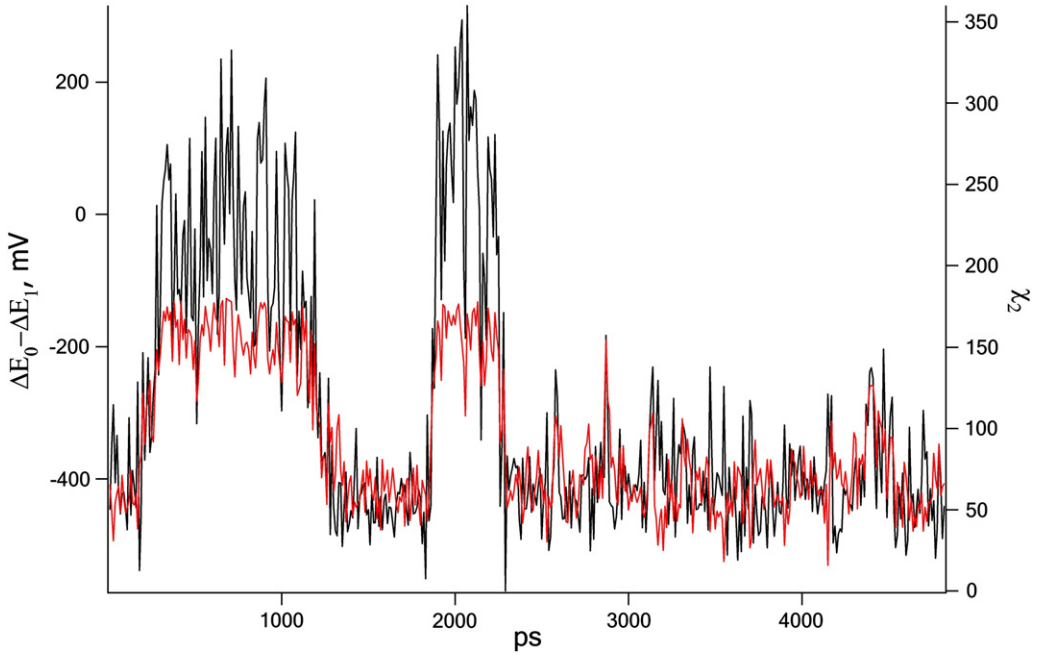

Fig. 5. Rotation of the Asn688$_{PsaA}$ residue along the angle χ_2 (red) and corresponding changes of the difference between electrostatic potentials at A_0 and A_1 (black), as measured on a 5 ns trajectory in the M688N$_{PsaA}$ variant in the A_0^- state.

As seen from Figs. 6 to 7, the total effect of Asn rotation by 110° on the gap between A_0 and A_1 potentials calculated by QC approach is ~820 meV, which is 2.2 times larger than the respective electrostatic effect of this transition, calculated previously by MD. This means that the proper contribution of Asn688$_{PsaA}$/Asn668$_{PsaB}$ to the reorganization energy of secondary electron transfer might be obtained by multiplying the result of respective MD calculations (70 meV for Asn688$_{PsaA}$ or 130 meV for Asn668$_{PsaB}$) by the same factor to account for the chemical interactions.

It is worthwhile to emphasize that our DFT calculations in vacuum might significantly overestimate the effect of Asn on the redox potential of A_0 and A_1 because they do not take into consideration (i) the dielectric screening by the protein environment, and (ii) conformational changes of cofactors caused by their charging and by Asn rotation.

To estimate the possible range of errors in the quantum chemistry model, we calculated (i) the effect of Asn rotation on the redox potential of A_0 in different basis sets, from the minimal 6-31G to the middle 6-311G with diffuse *sp* shells added to heavy atoms, and (ii) the effect of a polar environment using the Polarizable Continuum Model.

Concerning the Basis Set Superposition Error (BSSE), we checked that the basis enlarging in the sequence 6-31G, 6-311G, 6-311G(d), and 6-311+G affected the range of ΔE_0 and ΔE_1 variation by less than 10%, which indicates the reliability of the values obtained. Apparently the BSSE is essentially reduced by a triple subtraction procedure used for the estimation of the Asn rotation effect on the redox potential changes. On the other hand, the influence of the dielectric environment (estimated by the Polarizable Continuum Model using chloroform in 6-311G basis set) decreased the range of ΔE_0 and ΔE_1 variations by approx. 30% and 50%, respectively. Chloroform was chosen because its dielectric constant of 4.81 is close to the calculated dielectric constant of the protein medium in the vicinity of RC [17]. However, since electronic polarization was not included in the MD calculations, the latter correspond better to QC calculations in vacuum.

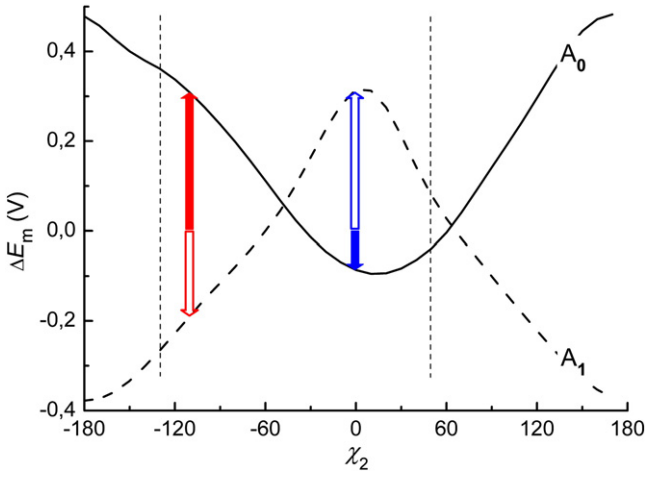

Fig. 6. Changes of chlorophyll A_0 and phylloquinone A_1 redox potentials caused by rotation of the Asn688$_{PsaA}$ residue in the variant, obtained by DFT calculations. Vertical dashed lines indicate the range of conformations observed in MD simulations. Redox potential changes of A_0 (filled arrows) and A_1 (open arrows) in two characteristic conformations of Asn observed in N/A_1^- (blue) and A_0^- (red) states are indicated. Redox potential of A_0 and A_1 in the wild type was taken as zero level.

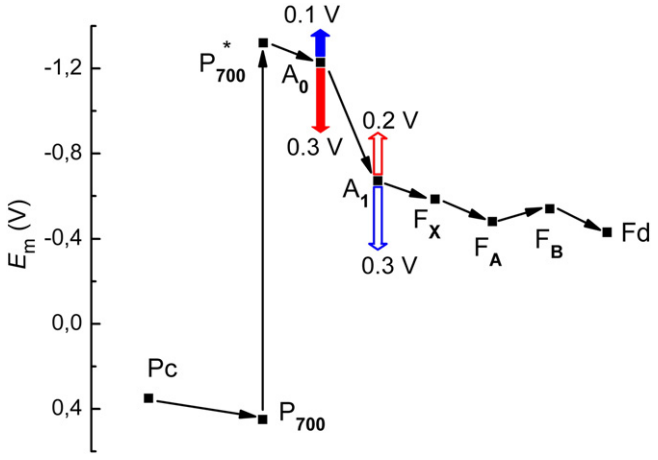

Fig. 7. Redox potentials of electron transfer cofactors in PS I. Redox potential changes of A_0 and A_1 are taken from Fig. 5 and designated by the same symbols.

3.6. Effect of Met➔Asn substitution and Asn rotation on the rate of secondary electron transfer

Secondary electron transfer from A_0 to A_1 could be affected by the conformation of Asn in different ways. If Asn remains fixed in the neutral conformation ($\chi_2 = 0$), the redox potential of A_1 will be raised by ~300 mV due to the effect of the amide group bonded to the C1 carbonyl oxygen of phylloquinone (the negative energy shift indicated by the blue filled arrow in Figs. 6 and 7). Alternatively, if Asn would be in the shifted position found for the state A_0^- ($\chi_2 = -100°/\chi_2 = +110°$), then the redox potential of A_1 will be lowered by 150 mV (the open red arrows in Figs. 6 and 7). Together with the 250 mV increased redox potential of A_0, this decreases the energy gap of the $A_0^-A_1$➔$A_0A_1^-$ transition ΔG_2 by 400 meV. Because the energy gap of this transition in wild type PS I is 500 to 600 meV [17], secondary electron transfer might be decelerated in such a rotated conformation of Asn, even if it is not tightly coupled with the back rotation of Asn to the basic position ($\chi_2 = 0$).

Bearing this in mind, it seems probable that primary charge separation occurs without rotation of Asn, but the latter might take place during the lifetime of the A_0^- state. The redox potential difference between A_0 and A_1 in wild-type PS I was estimated to be 560 mV for branch *A* and 470 mV for branch *B* [17], hence the change of ΔG_2 by the Asn rotation is not enough to block secondary transfer completely, and the effect of Asn should be included in both ΔG and λ terms of the Marcus Eq. (1).

In wild type PS I, the outer-sphere part of the reorganization energy in secondary charge separation obtained by MD calculations was ~450 meV. If we include the internal reorganization of the cofactors, which can be as high as 110–150 meV [30,31], the total λ_2 value would be about 560–600 meV, which is rather close to the ΔG_2 value of −560 meV determined previously for branch *A* [17]. Such a matching is consistent with the temperature-independent nature of the secondary electron transfer reaction in wild type PS I.

The dependence of the kinetics of the A_0➔A_1 electron transfer reactions on the energetic characteristics (ΔG_2 and λ_2) was described in PS I previously [33]. The problem is complicated by the intricate mechanics of electron transfer in the heterogeneous medium of the photosynthetic RC and by the uncertainty in the estimation of the E_m values of the cofactors used in the earlier studies. Iwaki et al. [33] considered the ΔG_2 of the A_0^-➔A_1 electron transfer to be −340 mV. On the basis of the rate constant dependence on ΔG_2 for different foreign quinones in the A_1 site, the total reorganization energy λ was found to be ~300 meV, whereas more recent studies suggest a ΔG_2 value as high as −560 mV [17], which is close to the calculated value of the reorganization energy λ_{out} (see Table 1). The same approach was applied earlier for estimation of λ for the similar electron transfer reaction in the bacterial RC (i.e. from bacteriopheophytin to Q_A) [34]. It is notable that the value of the reorganization energy obtained in [34] (600 ± 100 meV) was similar to the λ_2 value of the A_0^-➔A_1 reaction for PS I obtained in this study.

The maximal possible influence of Asn rotation on the energy of the primary and secondary charge separation reactions is summarized by the diagram in Fig. 7. The energy levels of different redox states in wild type PS I are shown as black lines. The energy shifts due to the Met to Asn substitution in the conformation of Asn fixed in its initial position ($\chi_2 = 0$) are shown by blue arrows, whereas red arrows correspond to the conformation in which Asn residue rotates to its optimal position in the A_0^- state ($\chi_2 = -100°/\chi_2 = +110°$).

The effect of the Met to Asn substitution on the rate of secondary electron transfer was calculated using the Marcus Eq. (1). To account for Asn interactions with A_0 and A_1, we used the linear interpolation and multiplied the contribution of Asn to the reorganization energy of secondary electron transfer by a factor of 2.2, calculated above (Section 3.5), which increased the total λ_2 from 695 to 780 meV (see Table 1). Regarding ΔG_2, we used the values of the A_0 and A_1 redox potentials for the wild type PS I from [17] and estimated the corresponding changes caused by Met➔Asn substitution from the changes of electrostatic potentials of A_0 and A_1, calculated by MD. ΔG_2 in $M688N_{PsaA}$ and $M668N_{PsaB}$ variants was lowered by 430 mV and 270 mV, respectively. These λ_2 and ΔG_2 changes are not sufficient to account for the experimentally observed slowdown of the secondary electron transfer in the PS I variants in the framework of Marcus theory.

The QC calculations (Section 3.5) demonstrate that the MD simulations cannot properly estimate the Asn interaction with cofactors, which determines the rate of its rotation. Therefore, the rotation of Asn in the PS I variants could be faster than the rate of electron transfer. In the latter case, the significant energy changes caused by Asn residue rotation (see Fig. 5 and Section 3.5) would account for the retarded electron transfer in the $M688N_{PsaA}$ mutant. Thus, the effects of such complex conformational movements could not be treated quantitatively neither by MD nor by QC alone, but the combined approach [15], applied in this study, might yield valuable results.

Our calculations of energetic effects of Met➔Asn substitution in the symmetrical cofactor branches gave rather similar results. However, our unpublished data indicate that electron transfer in each branch occurs independently, resulting in the primary charge separation reaction $(P_{700}A_0)^*$➔$P_{700}^+A_{0A}^-$ or $(P_{700}A_0)^*$➔$P_{700}^+A_{0B}^-$. The contribution of branch *B* was estimated to be ~30% [35], making it difficult to resolve this kinetic component in ultrafast kinetic experiments [12]. This asymmetry might be caused by the 40 mV difference in redox potentials of A_{0A}/A_{0B}, as estimated by the SC model published previously [17]. Other factors might include (i) a different flexibility of the protein matrix in the vicinity of A_0 and A_1 in the *A* and *B* branches (demonstrated by different numbers of shifted atoms in Fig. 2 and the opposite direction of rotation of axial ligand in Fig. 4B); (ii) the asymmetric orientation of tightly bound water as demonstrated by MD (see Section 3.4); and (iii) asymmetric effects of charged amino acids on the redox potentials of A_{1A}/A_{1B} as obtained by the SC approach in [17].

The transition of Asn between rotamers in the $M688N_{PsaA}$/$M668N_{PsaB}$ variants was observed on average once every ~1 ns (in 20-ns long MD trajectories), which is approximately an order of magnitude slower than the lifetime of the A_0^- redox state in the $M688N_{PsaA}$ variant [12]. Hence, only a partial propagation of the Asn rotamer distribution from its narrow shape in the N state to the wide distribution in the A_0^- state (Fig. 4) might occur within the lifetime of the A_0^- redox state in the PS I variants. We indeed observed the Asn rotamer changes in ~10% of 100 ps trajectories; however, minor details of PS I structure may significantly affect the rate and nature of such rotamer changes (as demonstrated by opposite directions of Asn rotation in the $M688N_{PsaA}$ and $M668N_{PsaB}$ variants). Therefore, the probability of Asn rotation (and the subsequent slowing of the secondary electron transfer) is proportional to two factors: the probability of primary electron transfer through the mutated branch (~70% in branch *A* and ~30% in branch *B*) and the frequency of Asn conformational changes in A_0^- state in the PS I variants.

An investigation of electron transfer in the $M688H_{PsaA}$/$M668H_{PsaB}$ variants of PS I demonstrated that substitution of Met by His blocks electron transfer from A_1^- to F_X in the respective branch [35]. The changes of redox potential of A_1 caused by Met➔Asn substitution and subsequent Asn rotation, as shown in Fig. 6, may rationalize this observation.

The obtained results indicate that a single amino acid mutation in the immediate surroundings of the electron transport chain cofactors can significantly affect the energetics of charge separation. The increased reorganization energy signifies a higher activation energy of charge separation in the variants, which in turn slows down the rate of these reactions. These results were practically symmetrical with regard to the two branches. It can therefore be concluded that the decrease in the experimentally observed secondary electron transfer rate in the $M688N_{PsaA}$ variant is caused primarily by a change in the redox potentials of chlorophyll A_0 and phylloquinone A_1, and by reorganization energy changes due to $Asn688_{PsaA}$ rotation to a conformation parallel to the chlorophyll plane, induced by primary charge separation.

4. Conclusions

1. A combined model of PS I from the cyanobacterium *T. elongatus* was created by consideration of data on three levels of approximation — classical molecular dynamics (protein as a whole), semi-continuum dielectric approach (effects of dielectric environment), and quantum chemistry calculations (local ligand–cofactor interactions).
2. A structural flexibility map of PS I based on MD simulations demonstrated that the hydrophobic core surrounding the primary redox cofactors is rigid, while the peripheral regions are much more flexible.
3. The atom shifts in the neighborhood of P_{700}, A_0 and A_1 caused by primary and secondary charge separation reactions were analyzed. By comparing the protein response to electron transfer in branches *A* and *B* of the wild type, we found that atom shifts of more than 0.5 Å in branch *B* caused by two consequent electron transfer reactions were ~1.5 times more numerous than in branch *A*, indicating a greater mobility of protein in the vicinity of branch *B*. The replacement of Met by Asn in any of the branches induced additional atom shifts in response to charge separation.
4. A combination of MD and SC approaches was used to estimate the reorganization energies (λ) of the primary (λ_1) and secondary (λ_2) charge separation reactions, which were found to be independent on the active branch of electron transfer; in wild type PS I, λ_1 was estimated to be 390 ± 20 mV, while λ_2 was estimated to be 445 ± 15 mV.
5. The combined approach, including DFT calculations, allowed an estimation of the effects of $Met688_{PsaA}$/$Met668_{PsaB}$ substitution by $Asn688_{PsaA}$/$Asn668_{PsaB}$ on the energetics of electron transfer. Unlike Met, which has a limited degree of freedom in the site, Asn was found to switch between two relatively stable conformations, depending on the charge state of the cofactor.
6. The introduction of Asn and its conformational flexibility significantly affected the reorganization energy of charge separation and the redox potentials of chlorophylls A_{0A}/A_{0B} and phylloquinones A_{1A}/A_{1B}, which may explain the experimentally observed slowdown of secondary electron transfer in the $M688N_{PsaA}$ variant.

Supplementary data to this article can be found online at http://dx.doi.org/10.1016/j.bbabio.2014.03.001.

Acknowledgements

This work was supported by grants from the Russian Foundation for Basic Research (RFBR 12-04-00821, HK-11-04-91330, HK-13-04-40299-H), the US National Science Foundation (MCB-1021725), and the Civilian Research and Development Foundation (CRDF RUB1-7029-MO-11).

References

[1] J.H. Golbeck, D.A. Bryant, Photosystem I, Curr. Top. Bioenerg. 16 (1991) 83–177.
[2] P. Jordan, P. Fromme, H.T. Witt, O. Klukas, W. Saenger, N. Krauß, Three-dimensional structure of cyanobacterial photosystem I at 2.5 Å resolution, Nature 411 (2001) 909–917.
[3] N.V. Karapetyan, A.R. Holzwarth, M. Rögner, The photosystem I trimer of cyanobacteria: molecular organization, excitation dynamics and physiological significance, FEBS Lett. 460 (1999) 395–400.
[4] J. Deisenhofer, O. Epp, K. Miki, R. Huber, H. Michel, Structure of the protein subunits in the photosynthetic reaction center of, Nature 318 (1985) 19.
[5] H. Komiya, T.O. Yeates, D.C. Rees, J.P. Allen, G. Feher, Structure of the reaction center from *Rhodobacter sphaeroides* R-26 and 2.4. 1: symmetry relations and sequence comparisons between different species, Proc. Natl. Acad. Sci. U. S. A. 85 (1988) 9012–9016.
[6] M. Guergova-Kuras, B. Boudreaux, A. Joliot, P. Joliot, K. Redding, Evidence for two active branches for electron transfer in photosystem I, Proc. Natl. Acad. Sci. U. S. A. 98 (2001) 4437–4442.
[7] W. Xu, P.R. Chitnis, A. Valieva, A. van der Est, K. Brettel, M. Guergova-Kuras, et al., Electron transfer in cyanobacterial photosystem I II. Determination of forward electron transfer rates of site-directed mutants in a putative electron transfer pathway from A_0 through A_1 to F_X, J. Biol. Chem. 278 (2003) 27876–27887.
[8] I.V. Shelaev, F.E. Gostev, M.D. Mamedov, O.M. Sarkisov, V.A. Nadtochenko, V.A. Shuvalov, et al., Femtosecond primary charge separation in *Synechocystis* sp. PCC 6803 photosystem I, Biochim. Biophys. Acta Bioenerg. 1797 (2010) 1410–1420.
[9] O.M. Sarkisov, F.E. Gostev, I.V. Shelaev, V.I. Novoderezhkin, O.A. Gopta, M.D. Mamedov, et al., Long-lived coherent oscillations of the femtosecond transients in cyanobacterial photosystem I, Phys. Chem. Chem. Phys. 8 (2006) 5671–5678.
[10] R.A. Marcus, N. Sutin, Electron transfers in chemistry and biology, Biochim. Biophys. Acta Rev. Bioenerg. 811 (1985) 265–322.
[11] R.O. Cohen, G. Shen, J.H. Golbeck, W. Xu, P.R. Chitnis, A.I. Valieva, et al., Evidence for asymmetric electron transfer in cyanobacterial photosystem I: analysis of a methionine-to-leucine mutation of the ligand to the primary electron acceptor A_0, Biochemistry 43 (2004) 4741–4754.
[12] N. Dashdorj, W. Xu, R.O. Cohen, J.H. Golbeck, S. Savikhin, Asymmetric electron transfer in cyanobacterial photosystem I: charge separation and secondary electron transfer dynamics of mutations near the primary electron acceptor A_0, Biophys. J. 88 (2005) 1238–1249.
[13] A.Y. Semenov, M.D. Mamedov, J.H. Golbeck, V.A. Shuvalov, V.A. Nadtochenko, Primary electron transfer reactions in Photosystem I complexes, in: Y.M. Feyziyev, I.M. Huseinova, S.I. Allakhverdiev (Eds.), Abstracts of International Conference "Photosynthesis Research for Sustainability", Nurlar, Baku, 2013, p. 79.
[14] A. Savitsky, O. Gopta, M. Mamedov, J.H. Golbeck, A. Tikhonov, K. Möbius, et al., Alteration of the axial Met ligand to electron acceptor A_0 in photosystem I: effect on the generation of P_{700}^{+} A_1^{-} radical pairs as studied by W-band transient EPR, Appl. Magn. Reson. 37 (2010) 85–102.
[15] A. Warshel, M. Levitt, Theoretical studies of enzymic reactions: dielectric, electrostatic and steric stabilization of the carbonium ion in the reaction of lysozyme, J. Mol. Biol. 103 (1976) 227–249.
[16] R.G. Alden, W.W. Parson, Zhen Tao Chu, A. Warshel, Orientation of the OH dipole of tyrosine (M)210 and its effect on electrostatic energies in photosynthetic bacterial reaction centers, J. Phys. Chem. 100 (1996) 16761–16770.
[17] V.V. Ptushenko, D.A. Cherepanov, L.I. Krishtalik, A.Y. Semenov, Semi-continuum electrostatic calculations of redox potentials in photosystem I, Photosynth. Res. 97 (2008) 55–74.
[18] W.D. Cornell, P. Cieplak, C.I. Bayly, I.R. Gould, K.M. Merz, D.M. Ferguson, et al., A second generation force field for the simulation of proteins, nucleic acids, and organic molecules, J. Am. Chem. Soc. 117 (1995) 5179–5197.
[19] M. Ceccarelli, P. Procacci, M. Marchi, An ab initio force field for the cofactors of bacterial photosynthesis, J. Comput. Chem. 24 (2003) 129–142.
[20] J.P. Perdew, K. Burke, M. Ernzerhof, Generalized gradient approximation made simple, Phys. Rev. Lett. 77 (1996) 3865.
[21] C. Adamo, V. Barone, Toward reliable density functional methods without adjustable parameters: the PBE0 model, J. Chem. Phys. 110 (1999) 6158.
[22] M.W. Schmidt, K.K. Baldridge, J.A. Boatz, S.T. Elbert, M.S. Gordon, J.H. Jensen, et al., General atomic and molecular electronic structure system, J. Comput. Chem. 14 (1993) 1347–1363.
[23] C.H. Chang, K. Kim, Density functional theory calculation of bonding and charge parameters for molecular dynamics studies on [FeFe] hydrogenases, J. Chem. Theory Comput. 5 (2009) 1137–1145.
[24] J.C. Phillips, R. Braun, W. Wang, J. Gumbart, E. Tajkhorshid, E. Villa, et al., Scalable molecular dynamics with NAMD, J. Comput. Chem. 26 (2005) 1781–1802.
[25] W. Humphrey, A. Dalke, K. Schulten, VMD: visual molecular dynamics, J. Mol. Graph. 14 (1996) 33–38.
[26] A. Nicholls, B. Honig, A rapid finite difference algorithm, utilizing successive over-relaxation to solve the Poisson–Boltzmann equation, J. Comput. Chem. 12 (1991) 435–445.
[27] E.L. Mertz, L.I. Krishtalik, Low dielectric response in enzyme active site, Proc. Natl. Acad. Sci. U. S. A. 97 (2000) 2081–2086.
[28] A.A. Granovsky, Firefly version 8.0.0, http://classic.chem.msu.su/gran/firefly/index.html.
[29] R. Ditchfield, W.J. Hehre, J.A. Pople, Self-consistent molecular-orbital methods. IX. An extended Gaussian-type basis for molecular-orbital studies of organic molecules, Chem. Phys. 54 (1971) 724.
[30] E. Sigfridsson, M.H.M. Olsson, U. Ryde, A comparison of the inner-sphere reorganization energies of cytochromes, iron–sulfur clusters, and blue copper proteins, J. Phys. Chem. B 105 (2001) 5546–5552.
[31] X. Amashukeli, N.E. Gruhn, D.L. Lichtenberger, J.R. Winkler, H.B. Gray, Inner-sphere electron-transfer reorganization energies of zinc porphyrins, J. Am. Chem. Soc. 126 (2004) 15566–15571.
[32] C.C. Moser, J.M. Keske, K. Warncke, R.S. Farid, P.L. Dutton, Nature of biological electron transfer, Nature 355 (1992) 796–802.
[33] M. Iwaki, S. Kumazaki, K. Yoshihara, T. Erabi, S. Itoh, ΔG^0 dependence of the electron transfer rate in the photosynthetic reaction center of plant photosystem I: natural optimization of reaction between chlorophyll *a* (A_0) and quinone, J. Phys. Chem. 100 (1996) 10802–10809.
[34] M.R. Gunner, P.L. Dutton, Temperature and $-\Delta G^0$ dependence of the electron transfer from BPh^- to Q_A in reaction center protein from *Rhodobacter sphaeroides* with different quinones as Q_A, J. Am. Chem. Soc. 111 (1989) 3400–3412.
[35] J. Sun, S. Hao, W. Xu, I. Shelaev, V. Nadtochenko, V. Shuvalov, et al., $M688H_{PsaA}$ and $M668H_{PsaB}$ variants of *Synechocystis* sp. PCC form a second H-bond to the A_{1A} and A_{1B} phylloquinones and a coordination bond to the A_{0A} and A_{0B} chlorophylls, Biochim. Biophys. Acta Bioenerg. (2014) (submitted for publication)